DOI: 10.31897/PMI.2019.2.133

UDC 550.394.4

REFINED ASSESSMENT OF SEISMIC MICROZONATION WITH A PRIORI DATA OPTIMISATION

Igor B. MOVCHAN, Alexandra A. YAKOVLEVA
Saint Petersburg Mining University, Saint-Petersburg, Russia

The work is devoted to the issues of seismic microzonation representativeness, which is amongst the mandatory assessments that precedes civil and industrial construction. In addition to the practical approach and in accordance with the normative documentation, the authors propose parametric interpretation of the remote basis by means of tracing geodynamic zones and elements of the geoblock structure, where the leading marker of seismogenic risk zones is the anomaly of spatial variability of the geofield, coinciding with the discordant intersection of localised land structures. Verification of this marker is achieved by displaying a cartographic distribution image within the range of the seismic point increment, detailed on the basis of approximation dependencies.

***Key words*:** seismic microzonation; upper part of the section; approximation; interpretation; remote basis; digital elevation model; geodynamic area

***How to cite this article*:** Movchan I.B., Yakovleva A.A. Refined Assessment of Seismic Microzonation With a Priori Data Optimisation. Journal of Mining Institute. 2019. Vol. 236, p. 133-141. DOI: 10.31897/PMI.2019.2.133

Introduction. A pronounced specialisation in the system of geophysical methods allows discussion on, particularly, a separate research direction related to engineering support of various production activities – from engineering and environmental surveys to industrial and residential construction. The specificity of this engineering geophysical support is regulated by the block of regulating acts RSN 66-87, 64-87 (Technical requirements for the production of geophysical works), which seemingly prescribe a deterministic methodology of field and laboratory work, as well as the structure of the reporting material, which should guarantee the representativeness of the results and the absence of significant claims from external expertise. In fact, the quality of engineering and geophysical work is determined by a set of factors leaving much to be criticised by an external expert. These factors include: limitation of the estimates of the investigated objects by field measurement materials while minimising post-processing; the rejection of the proven thesis about the integration of tool definitions. For example, when calculating the increment of seismic score [5] according to the Medvedev formula announced in standards, conditions far from the resonance of the layered thickness of the upper part of the section (UPS) when it is excited by an external seismogenic impulse, are considered. The standard estimate of seismic danger is reduced to the recalculation of rock density by a system of wells and data shallow seismic survey in the areal distribution of the increment of seismic intensity ΔI. In the best case, the expert observes the formation of distribution maps of the parameter ΔI, the maxima of which mark the areas of reduced stability of the UPS, and at worst – the average value of the increment of seismic scores throughout the declared polygon. Finally, the issue is to create a field work methodology and to perform the interpretative analysis of their results that can provide a representative assessment of the localisation and quantitative characteristics of areas of high seismic risk in the conditions of minimal provision of a priori field information.

Working methods. Within the framework of the formulated problems, the most effective is the complex of well testing with the methods of field geophysics (shallow seismic prospecting and electrotomography). The tasks traditionally include tracking a roof of the bearing horizon and assessment of the seismic score increment. If the first problem is associated with a deterministic structural-real complex, the second one is of a predictive nature [1]. The latter means the calculation of the parameter (here – ΔI), which is not checked either by full-scale testing of the rock mass, or by physical and mathematical modelling of its state, while marking only the potential reaction of the upper part of the section to dynamic seismogenic and static anthropogenic loads.

DOI: 10.31897/PMI.2019.2.133

Focusing on the most problematic second problem, we note the key methodological elements of its solution: a set of periodically updated maps of General seismic zoning (OSR series), developed on the basis of the methodology of V.I.Ulomov, V.N.Strakhov et al. [11]; regulatory documentation (for example, MDS 22.1-2004 «Guidelines for seismic microzonation...»). The basis of the normative numerical recalculation, as noted, is the analytical ratio of Medvedev

$$\Delta I = 1{,}67 \lg\left(\rho_{ref} \upsilon_{ref} / \left(\rho_{cur} \upsilon_{cur}\right)\right), \quad (1)$$

where the reference acoustic impedance is in the numerator under the logarithm (rock density ρ multiplied by velocity υ of elastic waves in them) for a given polygon, and the current acoustic impedance in a small neighborhood of instrumental testing is in the denominator.

When assessing the reference and actual acoustic stiffness, the recommendation is applicable to the calculation of the well column weighted average characteristics [4]:

$$\tilde{\rho\upsilon} = \sum_i \rho_i \upsilon_i \cdot h_i / \sum_i h_i ,$$

where h_i is the thickness of the i-th structural-real layer.

To link quantitative assessments to the geological basis, it is recommended to update it at the level of generalisation of archival data, as well as thematic interpretation of the remote data. To compensate for the approximate nature of the estimates according to the Medvedev's formula, the calculation of synthetic accelerograms is practiced, reflecting the reaction of the stratified thickness of the upper part of the section to a broadband seismogenic impulse. The operation consists in the numerical solution of the differential equation of damped forced harmonic oscillations

$$m\frac{d^2\xi}{dt^2} + c\frac{d\xi}{dt} + k\xi = -m\left(\frac{d^2\xi}{dt^2}\right)_g , \quad (2)$$

where m is the mass; ξ is the relative displacement of a single node of the nonequilibrium model; c is the viscous attenuation; k is the system stiffness.

The solution (2) can be found [13] in the frequency plane as well as in the subject plane on the basis of the numerical taking of the Duhamel's integral.

Development of methods. The first part of our research is related to the compensation of the expressed methodical defects. We consider classification and thematic interpretation of multispectral images as tools to follow-up geodynamic zones (GDZ) and to primary forecast risk zones under the reduced stability of the UPS areas (possible sources of earthquakes, PSE). The latter are considered as discordant areas of intersecting various ranked GDZs. Parametric morphostructural interpretation is based on the author's methodology of lineament-spectral analysis [14, 15], where the spectral channel of the remote basis is used, which has the greatest contrast for different ranges of the optical density field (1024 brightness gradations at 16-bit encoding; range sampling is performed in the vicinity of the maxima of the empirically accumulated distribution histogram). According to the chosen spectral channel, we trace algorithmically the thickening of linear landscape elements (lineaments), marking a GDZ, as well as areal objects of arbitrary morphology, marking natural-territorial complexes of a certain rank, sometimes, syngenetic elements of the geoblock structure.

GDZ mapping is done in two stages. The first involves digitising the optical density field of the most contrasting spectral channel of the remote base (usually the 5th channel, the wavelength range from 1.55 to 1.75 microns). The parametric lineament interpretation is executed with the digitised remote basis: determination of the position of extreme points in the optical density field $f(x, y)$ and in the module of its horizontal gradient $\left|\vec{\nabla} f\right| = \sqrt{(\partial f / \partial x)^2 + (\partial f / \partial y)^2}$; rotation relative to each extreme point with the coordinates (x_0, y_0) of the radius vector (elementary lineament) using the rotation matrix

DOI: 10.31897/PMI.2019.2.133

$$\begin{pmatrix}\tilde{x}\\ \tilde{y}\end{pmatrix}=\begin{pmatrix}\cos\alpha & \sin\alpha\\ -\sin\alpha & \cos\alpha\end{pmatrix}\cdot\begin{pmatrix}x-x_0\\ y-y_0\end{pmatrix}.$$

Along each point $(\tilde{x},\tilde{y})$ of the radius vector, the values of the processed component of the optical density field are selected algorithmically using spline interpolation [7]

$$f(\tilde{x})=(x_{i+1}-\tilde{x})^2(2(\tilde{x}-x_i)+h)f_i h^{-3}+(\tilde{x}-x_i)^2(2(x_{i+1}-\tilde{x})+h)f_{i+1}h^{-3}+$$

$$+(x_{i+1}-\tilde{x})^2(\tilde{x}-x_i)f_i' h^{-2}-(\tilde{x}-x_i)^2(\tilde{x}-x_{i+1})f_{i+1}' h^{-2}, \quad (3)$$

where $i=\text{int}[(\tilde{x}-a)/h]$; (x_i,x_{i+1}) are the coordinates of nearby nodes of the optical density field matrix; f_i and f_{i+1} are the values of the optical density at these nodes; f_i' and f_{i+1}' are the first derivative of the optical density at these nodes; $a = x_0$; h is the step between the nodes.

By means of the selection $f(\tilde{x})$ along the elementary lineament corresponding to the angle of its rotation α, we calculate the spatial variability of the optical density field as a function α, which at the end of the rotation gives the dispersion functional. Its minimum reflects the optimal orientation of the elementary lineament coinciding with the axis of the dominant stretch of the geomorphological anomaly or with the axis of the gradient zone. We determine the family of trend lines with the final calculation of the intersection points (x_0, y_0) (discordant positions) of these trends on the basis of Kramer's theorem and the solution of a system of two linear equations (to determine the ratio of linear approximations of trends).

Tracing of GDZs and localization of their discordant intersections are verified by mapping the geoblock structure of the polygon [6]. It is associated with the allocation of areas of spatial stationarity in the structure of the selected spectral channel of the remote base. The operation involves the calculation of the autocorrelation radius of the optical density field $f(x)$ over the entire area of the remote image based on the structure of the two-dimensional autocorrelation function (ACF). The estimation of the autocorrelation radius r by area gives an elliptical contour, the size and orientation of which determine the parameters of the sliding interval. For each position of the latter, a secondary selection of the optical density field value is carried out with repeated calculation in the moving interval of the mean radius of autocorrelation r, which plays the role of an integral parameter of variability of the amplitude-frequency composition of the remote base (landscape component) [10]:

$$r=0.5(R(0))^{-1}\int_{-\infty}^{+\infty}R(\tau)d\tau, \quad (4)$$

where $R(\tau)=\int_{-\infty}^{+\infty}f(x)f(x\pm\tau)dx$ is the autocorrelation function of the optical density field.

The boundaries of geoblocks are marked by the difference of the averaged parameter r within each geoblock, and the anomalous region (reduced stability of the UPS) is indicated by the maximum jump of the integral variability parameter [9] in a junction area of three or more geoblock boundaries.

The results of the parametric interpretation, the linear and areal objects with a forecast of local areas of seismic risk are verified by the assessment ΔI using the approximation of the functional relationship between density ρ of loose strata and speed of elastic waves in them (for example, according to empirical dependences [3]). In the case of the longitudinal wave velocity V_P measured in the stratified sedimentary column,

$$\rho=\frac{V_P\cdot10^{-3}+6.4}{4.0}, \quad (5)$$

where $V_p=(5.45\exp((\rho-2.60)/2.00)\pm0.50)\cdot10^{-3}$; V_P is measured in meters per second; ρ is measured in grams per cubic centimetre.

DOI: 10.31897/PMI.2019.2.133

Such recalculation in the application of the Medvedev's formula allows to limit the volume of seismic estimates in the presence of only core testing data and vice versa. To detail the image of the spatial distribution calculated according to parameter (1) ΔI, we implement the selection of an analytical function that displays the functional relationship between the increment of seismic scores and the spatial gradient $\left|\vec{\nabla}H(x,y)\right|$ of the field of absolute heights of the Earth's surface:

$$\log_a \Delta I_\Sigma = c_i + d_i \log_a \left(\left|\vec{\nabla}H(x,y)\right|\right), \quad (6)$$

the logarithmic properties of which is verified on several experimental polygons corresponding to different geostructural conditions and geodynamic positions; the factors c_i and d_i are empirical.

Assessment of methods. The work was performed on the example of an industrial park project located in a potentially seismically active zone of one of the Russian southern regions. There are three structural levels in the vicinity of the polygon: folded complex (Triassic – Upper Jurassic), cover complex (Cretaceous – Eocene), and sinophorogenic alpine complex (elevated erosion relief and sinorogenic Oligocene sediments of the Quaternary period). They are formed under the conditions of cyclicity of transgressive-regressive dynamics, which determines the spatially regular nature of the network of discontinuous disturbances [9]. Laid on the first cycles of tectono-magmatic activation disjunctives have been repeatedly resuscitated until modern times, which has led to the development of the faults in all structural levels. The polygon map shows linear, radial and ring fractures, where the first has a predominantly North-West and North-East directions, forming quasi-periodical network with a strong shear kinematics, marked by the system of branch sigma-shaped faults. Radial and arc faults are confined to the structures of the central type corresponding to the breaks in the tensile environment.

Visual analysis of a detailed remote image of the study area allows finding developed man-made complexes, counter-balancing responses from the components of the natural landscape, which determines the primary trace of a GDZ at a scale of 1:100 000 (Fig.1, *a*). Herewith, a geodynamic zone is converted into a ranked map image, which includes the ring structure, the significance of which is the higher, the closer the centre of curvature of each circle-like structure located towards the discordant region of geodynamic zones. When ranking GDZs, the main criterion is their length (laying depth) and degree of fragmentation (age of the last activation). At the regional scale, we distinguish five ranks of geodynamic zones, the first of which corresponds to the least extended and

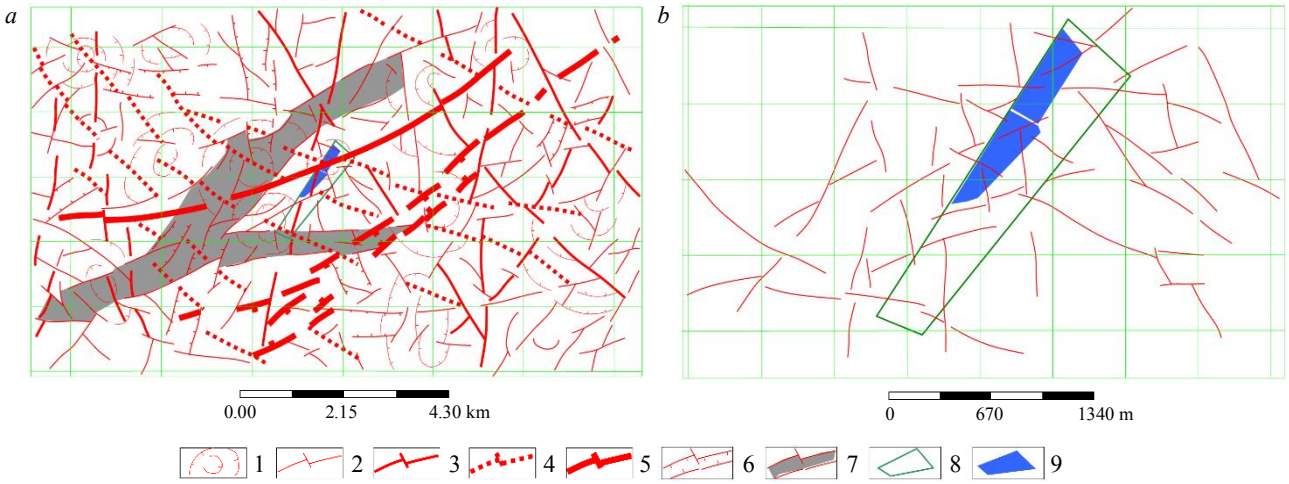

Fig.1. The result of thematic interpretation of the remote basis (RB) and digital elevation model (DEM) using the formula (3): *a* is for decoding on a regional scale; *b* is for large-scale tracking of a GDZ

1 is for ring structures; 2, 3, 4, 5, 7 are for geodynamic zones of the grades 1, 2, 3, 4 and 5, respectively; 6 is for the intermediate type of geodynamic zones, which are organised into local strip-like formations of a given stretch azimuth; 8 is for the fundamental binding to the field of engineering study; 9 is for the contour of cultivated fields
(element of spatial linking of different-scale materials)

DOI: 10.31897/PMI.2019.2.133

most latent structures, and the fifth rank corresponds to GDZs, explicitly displayed in a modern landscape. PSE forecast areas correspond to discordants [12] in the southern, Central and Northern parts of the licensing circuit.

When performing the large-scale photointerpretation (scale 1:30 000, Fig.1, *b*), tracing of coaxial structures is possible due to the analysis of the landscape of the territories adjacent to the boundaries of a polygon. The objectivity of attribution of these structures to GDZs is provided by comparison with the result of regional interpretation: the PSE areas identified at all stages of photointerpretation tend to share the same positions.

At the stage of geoblock reconstruction (Fig.2) a detailed digital model of the Earth's elevations is applied: the complexity of the morphostructural image is associated with anthropogenic changes in the land topography, which is partially counter-balanced by tracing the extended lineament structures. A bergstrich is assigned to each geoblock boundary, pointing the direction of increasing terrain differentiation degree. According to the formula (6), areas of increased variability in the spatial gradient of the absolute height field are important for the primary prediction of PSE regions.

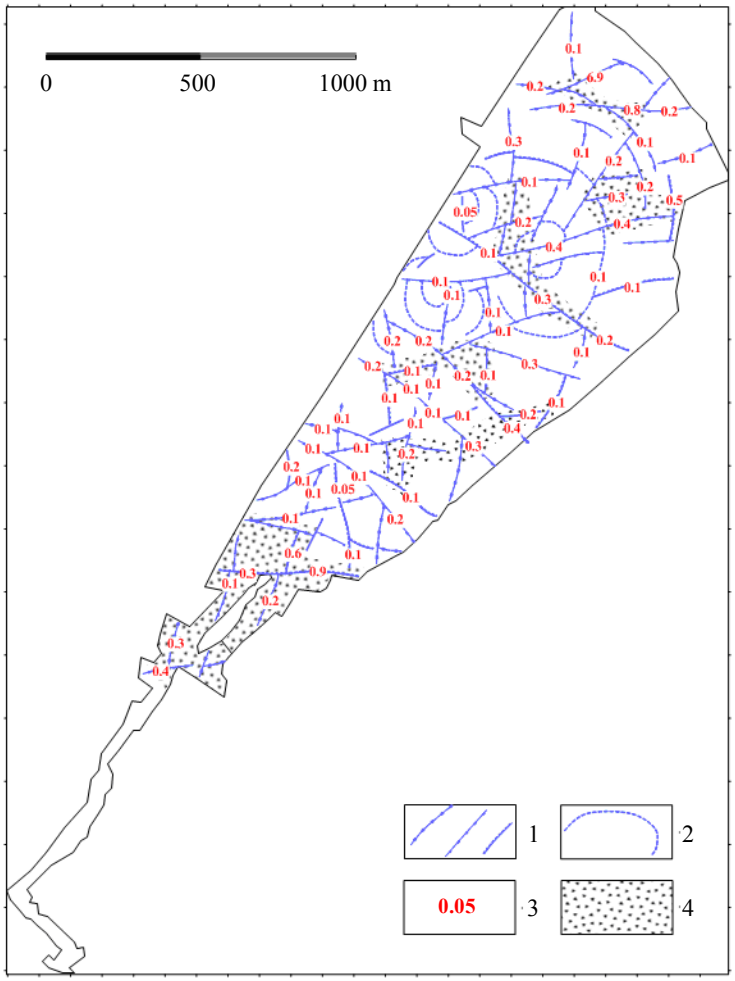

Fig.2. The result of geoblock boundary mapping on the basis of the formula (4) with their ranking within the field of engineering survey (Fig.1)

1 – borders with bergstrichs (indicating an area of higher variability of the DEM morphology); 2 – borders, reflecting verified ring structure; 3 – the normalised differential relief on the geoblock border; 4 – the forecast area of seismic risk according to the criterion of variability of the normalised parameter differential relief on geoblock borders (2 times and more)

Clarification of their position is implemented by means of quantitative estimates of seismic microzonation (SMZ).

The land topography of the studied area is complex, with a height difference of tens and first hundreds of metres, so landslide threats are possible. In addition, the reduced resistance of the UPS to external loads can be associated, firstly, with the position of the elements of the discontinuous tectonics, and secondly, with the water content of strata. The drilling results (Fig.3) show that the near-surface structural-material complexes are composed of loose sand-clay formations, which total thickness varies from the first tens of centimetres to the first metres, as well as of underlying weathered limestone.

In the two wells (the Southern polygon part) of the twenty-nine, a groundwater table has been found at a depth of $h \le 2$ m, which gives a significant increment of seismic scores in accordance with the approximation dependence of the type (according to [1])

$$\Delta I_{\text{GWT}} = K \exp\left(-0.04h^2\right) = 0.95 \exp\left(-0.04(1.50)^2\right) = 0.87 ,$$

where $K = 0.95$ is an empirical factor; GWT is an adjustment factor taking into account the level of the groundwater table.

a

Absolute height of the mouth: 218.4 m

Geological age	Bottom depth, m	Absolute height, m	Strata thickness, m	Lithological section	Rock description	Water appearance, m	Stable water level, m
b Qh	0.1	218.26	0.1		Soil and vegetation layer		
e Q	0.5	217.86	0.4		Sandy clay loam Sandy clay concrete subsidental loam with rotted rocks and gravel up to 25 %, with calcareous spots; grey, brown $\rho_{weighted\ mean}$ = 1.7 g/cm^3		
P2	5.0	213.36	4.5		Low-strength limestone with marl layers, dense softened, fractured, weathered in the roof; grayish-white $\rho_{weighted\ mean}$ = 2.01 g/cm^3		Groundwater is not found

Scale 1:100

b

Absolute height of the mouth: 170.3 m

Geological age	Bottom depth, m	Absolute height, m	Strata thickness, m	Lithological section	Rock description	Water appearance, m	Stable water level, m
b Qh	0.1	170.15	0.1		Soil and vegetation layer		
t Qh	2.5	167.75	2.4		Bulk soil: loam with pebbles, gravel, sand layers and admixture of construction debris (brick fragments, broken glass); gray-brown $\rho_{weighted\ mean}$ = 1.68 g/cm^3	1.5	1.6
a Qh	110				Sandy light loam (light loam) fluid-plastic, with interlayers of fluid sandy loam; light gray $\rho_{weighted\ mean}$ = 1.93 g/cm^3		

Scale 1:100

Fig.3. Excerpts from drilling results, reflecting the monotonous occurrence nature of rocks in the upper part of the section: *a* – an example of a column to a depth of 5 m in wells in the Northern and Central parts of the polygon (groundwater is not found); *b* – an example of a column to a depth of 11 m in the well in the Southern part of the polygon (groundwater is found at a depth of less than 2 m)

ρ_{weight} – laboratory determination of the weighted average density verification according to the formula (5) for individual layer

In the rest of the wells, groundwater is not found at a ten-metre depths. According to the studied borehole columns within the polygon (Fig.3), the initial sample is formed for the weighted average section, which upper layer consists of loam with rotted rocks, and the lower layer is composed by weathered limestone. A group of southern wells is exceptional, as the top layer is formed there by bulk soils, and the underlying substrate is represented by loams of different consistency. We consider a virtual structural-real complex as a reference layer; its acoustic stiffness is taken as a weighted average for all open drilling and verified seismic complexes within the study area: $(\rho V_P)_{ref} = 2.28 \cdot 10^{-3}$ g/s, $(\rho V_S)_{ref} = 1.56 \cdot 10^{-3}$ g/s.

DOI: 10.31897/PMI.2019.2.133

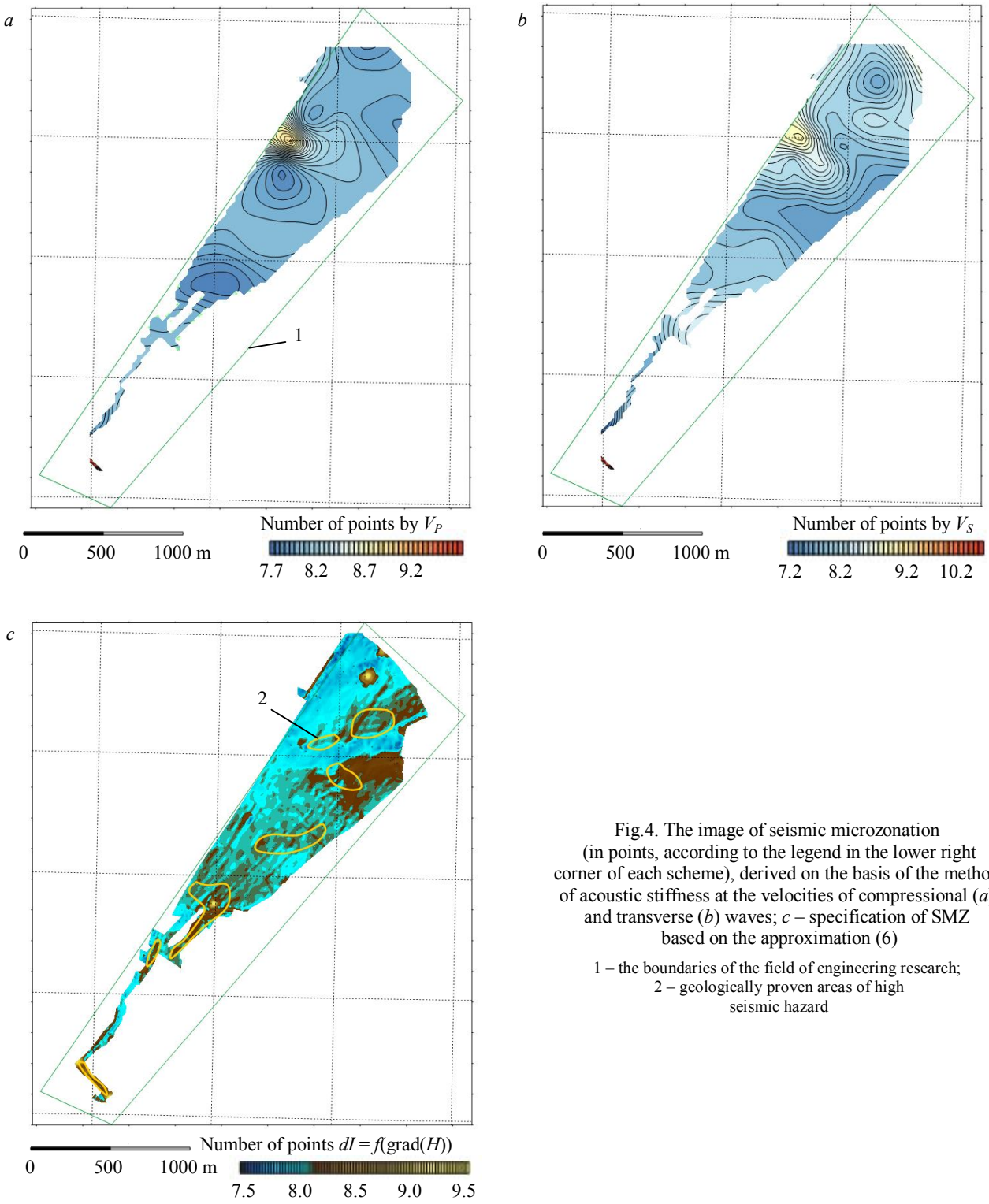

Fig.4. The image of seismic microzonation (in points, according to the legend in the lower right corner of each scheme), derived on the basis of the method of acoustic stiffness at the velocities of compressional (*a*) and transverse (*b*) waves; *c* – specification of SMZ based on the approximation (6)

1 – the boundaries of the field of engineering research; 2 – geologically proven areas of high seismic hazard

By adding the final increments ΔI to the most probable number of points equal to eight (derived from the OSR-2015 maps), and continuing with the spatial distributions, we obtain a system of area images (Fig.4, *a*, *b*). A spatial image of the polygon SMZ, drawn by shear wave velocities, shows the best correlation between positive extrema and PSE areas localised at a qualitative level by the analysis of RB and DEM, compared to SMZ based on compressional waves. Zoning based on recalculations of compressional and transverse velocities verify each other and confirm the thesis of the greatest significance of PSE areas that are situated in the Northern and Southern parts of the study area. Trying to detail the obtained schemes of seismic points distribution, we use approximation (6), which in our case takes the form

DOI: 10.31897/PMI.2019.2.133

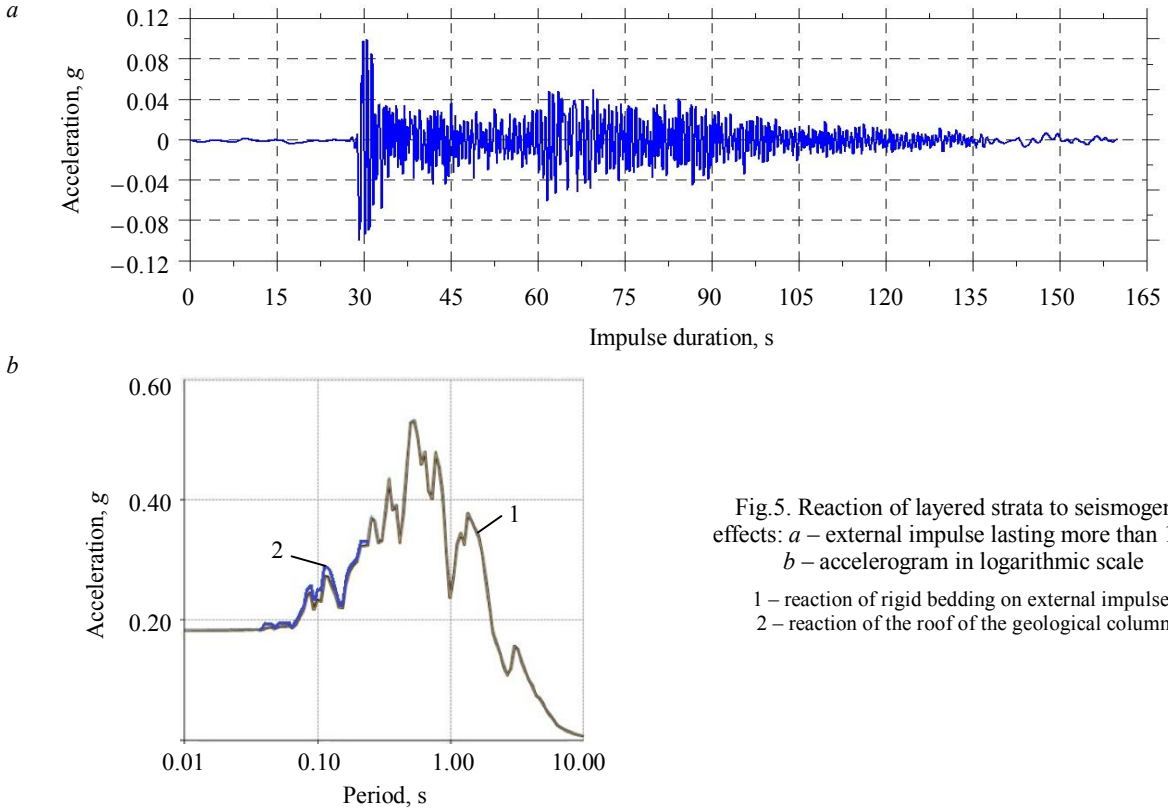

Fig.5. Reaction of layered strata to seismogenic effects: *a* – external impulse lasting more than 120 s; *b* – accelerogram in logarithmic scale

1 – reaction of rigid bedding on external impulse;
2 – reaction of the roof of the geological column

$$\ln(I) = 0.02843 \ln\left(\left|\vec{\nabla} H\right|\right) + 2.16752 .$$

From the point of view of mathematical physics such recalculation represents no more than rationing of a spatial gradient field of heights of the land topography (Fig.4, *c*). From the point of view of physics, the spatial gradient of these heights is associated with the response of a local area to endogenous seismological effects: elevation changes mark the dynamics of compression-tension load on the underlying geological substrate, and relatively steep slopes can be considered as potentially dangerous in terms of tangential soil displacements.

According to normative estimates [8], the number of points within the studied object varies in the range of 7-8 points, which means the amplitude of the initial impulse acceleration of the order (0.05-0.15)g (where g is the acceleration of gravity). The impulse duration in our model is 120 s and its broadband composition allows the resonance state of the stratified geological environment (Fig.5, *a*).

The synthetic accelerogram is shown in Fig.5, *b*, where the background of the primary impulse accelerogram (bold brown curve) reflects the spectral response from the roof of each of the rock complexes embedded in the original model.

The low-amplitude reaction of the single-layer medium is obvious; it is a slight increase in vibration acceleration in the vicinity of the period from 0.1 s with an excess of no more than 0.05g in the maxima. In the framework of such estimates, we determine the periods of natural oscillations T of the studied elastic system, which in the first approximation is realised on the basis of the ratio

$$\cos(\omega h / V_S) = 0 \quad \text{or} \quad T = 2\pi/\omega = 4h/(kV_S) \quad \text{at} \quad k = 1; 3; 5; \ldots,$$

where ω is the cyclic frequency, $\omega = 2\pi f = 2\pi / T$; $k/4 = h/\lambda = h/(TV_S)$, odd values of k correspond to spectral peaks; λ is the wavelength.

So for the upper layer period $T = 0.03$; 0.016 s, etc. The value of the natural oscillation period $T = 0.03$ s is beyond the formation of peaks in the spectral response of the layered medium to the external elastic action. Thus, we can assume the absence of resonance in this case and the correctness of the estimates according to the Medvedev's formula.

DOI: 10.31897/PMI.2019.2.133

Conclusions are presented by methodical and approbation parts:

1) normative quantitative assessments of seismogenic risk in the field of construction of engineering structures are linear in nature, and therefore cannot give the final idea of the position, quantitative characteristics of risk areas and require instrumental and office additions;

2) in the instrumental part it is recommended to integrate methods of borehole testing and field geophysics (seismic and electric prospecting) at uniform coverage of a polygon with measurement points and accompanied by remote sensing for the purpose of representative allocation of sites of growing seismic levels and verification of these sites when mapping GDZs and PSE zones;

3) if it is impossible to implement paragraph 2, a combination of parametric and expert approaches is effective in the thematic interpretation of the remote basis of small and large scales, as well as the DEM, aimed at tracing the GDZs, mapping elements of the geoblock structure and, finally, verified forecast of PSE zones;

4) approximation dependences associated with the mutual recalculation of the density and velocities of elastic waves, as well as the calculation of seismic levels based on the data of topogeodesic surveys and the depth of the groundwater table, are a workable tool to improve the degree of SMZ detail in a limited sample of field measurements; it is necessary to pay attention to the need to verify the empirical factors of these dependences within the test polygons;

5) for the long-term development of the assessment of the resonance response of the UPS to the seismogenic impulse, the method of calculating synthetic accelerograms and natural oscillations can be supplemented by the use of the Medvedev's formula on the axis of the column depths of each well, as by physical, mathematical or analogue modelling of dangerous landslide processes at complicated land topogrphy or processes of karst gravitational collapse.

REFERENCES

1. Aleshin A. S. Seismic microzoning of highly sensitive objects. Moscow: Svetoch Plyus, 2010, p. 303 (in Russian).
2. Gzovskii M.V. Mathematics in geotectonics. Moscow: Nedra, 1971, p. 240 (in Russian).
3. Magid M.Sh. Petrophysical characteristics of the lithosphere and mantle. Petrofizika. Zemnaya kora i mantiya: Spravochnik. Pod red. N.B.Dortman. Moscow: Nedra, 1992, p. 221-225 (in Russian).
4. Maksimov A.B. On the seismic impedance of the soil. Eksperimental'naya seismologiya. Moscow: Nedra, 1971, p. 240 (in Russian).
5. Medvedev S.V. Engineering seismology. Moscow: Stroiizdat, 1962, p. 284 (in Russian).
6. Movchan I.B., Yakovleva A.A. The method of structural and morphological zoning on the example of N-38 map sheet. *Zhurnal nauchnykh publikatsii aspirantov i doktorantov*. 2016. N 4 (118). 2016. p. 167-169 (in Russian).
7. Mudrov A.E. Numerical methods for PC in the languages BASIC, FORTRAN and PASCAL. Tomsk: MP «Rasko», 1992, p. 272 (in Russian).
8. General seismic zoning of the territory of the Russian Federation: Explanatory note to the set of maps OSR-2016 and a list of settlements located in seismic zones. Pod red. V.I.Ulomova, M.I.Bogdanova. *Inzhenernye izyskaniya*. 2016. N 7, p. 121 (in Russian).
9. Petrov O.V., Movchan I.B. Applied aspects of the theory of dissipative non-equilibrium structuring of the geological medium. Dissipativnye struktury Zemli. St. Petersburg: Izd-vo VSEGEI, 2007, p. 202-267 (in Russian).
10. Serkerov S.A. Spectral analysis in gravity and magnetic exploration. Moscow: Nedra, 1991, p. 279 (in Russian).
11. Ulomov V.I., Shumilina L.S. The problem of seismic zoning in Russia. Moscow: Vserossiiskii NII problem nauchno-tekhnicheskogo progressa i informatsii v stroitel'stve, VNIINTPI Gosstroya Rossii, 1999, p, 42 (in Russian).
12. Khesin B.E., Alekseev V.V., Metaksa Kh.P. Interpretation of magnetic anomalies in conditions of oblique magnetization and rugged topography. Moscow: Nedra, 1983, p. 288 (in Russian).
13. Matasovic N. Seismic response of composite horizontally-layered soil deposit: Ph.D. Thesis. Univ.of California, LA, USA. 1993, p. 235.
14. Movchan I.B., Yakovleva A.A. Experience of qualitative and quantitative interpretation of nonpotential geofields with surface and deep morphostructural reconstructions on the example of Unica ore province (Kareljya, Russia). *International Journal of Mechanical Engineering and Technology* (*IJMET*). 2017. Vol. 8. Iss. 12, p. 926-932.
15. Movchan I.B., Kirsanov A.A., Yakovleva A.A. Qualitative interpretation of remote sensing materials in environmental and geological problems. *World Applied Sciences Journal*. 2014. Vol. 30(1), p. 39-45.

***Authors*: Igor B. Movchan,** *Candidate of Geological and Mineralogical Sciences*, *Associate Professor*, *Movchan_IB@pers.spmi.ru* (*Saint-Petersburg Mining University*, *Saint-Petersburg*, *Russia*), **Alexandra A. Yakovleva,** *Candidate of Physical and Mathematical Sciences*, *Associate Professor*, *Yakovleva_AA@pers.spmi.ru* (*Saint-Petersburg Mining University*, *Saint-Petersburg*, *Russia*).

The paper was received on 18 Yanuary, 2019.
The paper was accepted for publication on 11 March, 2019.